DEPARTMENT OF THE NAVY

HYDROMECHANICS

o

AERODYNAMICS

o

STRUCTURAL MECHANICS

o

APPLIED MATHEMATICS

o

ACOUSTICS AND VIBRATION

THE EFFECT OF INITIAL IMPERFECTIONS ON THE COLLAPSE STRENGTH OF DEEP SPHERICAL SHELLS

by

Martin A. Krenzke and Thomas J. Kiernan

40p

STRUCTURAL MECHANICS LABORATORY
RESEARCH AND DEVELOPMENT REPORT

February 1965 Report 1757

37p

THE EFFECT OF INITIAL IMPERFECTIONS ON THE COLLAPSE STRENGTH OF DEEP SPHERICAL SHELLS

by

Martin A. Krenzke and Thomas J. Kiernan

February 1965

Report 1757

TABLE OF CONTENTS

LIST OF FIGURES

LIST OF TABLES

ABSTRACT

An analysis is developed to account for the effects of imperfections on the collapse strength of spherical shells. The analysis is empirical but is based on an engineering evaluation of recent tests of near-perfect deep spherical shells and spherical caps. Sixty-two models were machined with local thin spots and flat spots and subjected to external hydrostatic pressure. The analysis is in good agreement with experimental results despite the severity of imperfections selected to test the analysis. The limitations of the analysis are discussed and curves showing the relationship between out of roundness and local radius are presented to aid the design engineer in establishing acceptable tolerance limits for fabrication of spherical shells.

ADMINISTRATIVE INFORMATION

The work described in this report was conducted under the Model Basin in-house independent research program, Project S-R011 01 01.

INTRODUCTION

The use of spherical shells to resist uniform external hydrostatic pressure has increased rapidly in recent years. This increased use results from the introduction of missiles and other spacecraft and also from the growing interest in hydrospace.

During the past three years, the David Taylor Model Basin has spent considerable effort developing design criteria for deep* spherical shells for hydrospace applications. This effort is primarily experimental. Machined specimens and specimens manufactured according to feasible large-scale fabrication procedures are being tested. The effect of initial imperfections, residual stresses, boundary conditions, stiffening systems, and penetrations on elastic and inelastic behavior are being studied.

It became evident early in the program that the collapse strength of deep spherical shells was critically dependent upon the presence of

---

*Here a deep spherical shell is contrasted to a shallow spherical shell whose height is normally assumed to be less than one-eighth of its base radius.

initial imperfections, primarily departures from perfect sphericity. However, no theory or design procedures could be found in the literature which adequately considered the effects of imperfections on either elastic or inelastic behavior. Furthermore, the magnitude of initial imperfections in the test specimens was not measured to the degree of accuracy required to evaluate the effects on collapse strength.

Because of this lack of design tools with which the designer could rationally determine the required geometries for practical deep spherical shells, the Model Basin developed a semi-empirical method for designing and analyzing initially imperfect spheres. This "engineering type" analysis is presented in this report together with the test results of machined models designed to investigate its adequacy.

BACKGROUND

Timoshenko[1] summarizes the classical small-deflection theory for the elastic buckling of a complete sphere as first developed by Zoelly in 1915. This analysis assumes that buckling will occur at that pressure which permits an equilibrium shape minutely removed from the perfectly spherical deflected shape. The expression for this classical buckling pressure p_1 may be given as

$$p_1 = \frac{2\,E\,(h/R)^2}{\sqrt{3\,(1-\nu^2)}} = 1.21\,E(h/R)^2 \text{ for } \nu = 0.3 \qquad [1]$$

where E is Young's modulus,

h is the shell thickness,

R is the radius to the midsurface of the shell, and

ν is Poisson's ratio.

Unfortunately, the very limited data available prior to the current Model Basin program do not support the linear theory; elastic buckling loads of roughly one-fourth those predicted by Equation [1] were observed in earlier tests recorded in the literature.[2] Various investigators have attempted

---

[1]References are listed on page 33.

to explain this discrepancy by introducing nonlinear, large deflection shell equations. In effect, their expressions for the theoretical buckling pressures resulting from the nonlinear equations take the same general form as Equation [1]. However, the elastic buckling coefficients corresponding to the minimum pressure required to keep an elastic shell in the post-buckling position are often about one-fourth of the classical coefficient and thus are generally in fair agreement with the early experiments. A more complete background on these large deflection analyses is given in References 2 and 3.

The test specimens used in the earlier tests,[2,4] the results of which have frequently been compared to the theoretical buckling pressures for initially perfect spheres, were formed from flat plates. Thus, although little data are available, it can be assumed that these early specimens had significant departures from sphericity as well as variations in thickness and residual stresses. Those specimens which were not complete spheres also had adverse boundary conditions. Since initial imperfections affect collapse strength, the comparison of existing theory, both linear and nonlinear, with the early experiments is not valid. Until recently,[5,6] however, no attempt has been made to theoretically evaluate the effect of initial imperfections on the collapse strength of deep or complete spheres.

The large discrepancy between the classical buckling pressure and the existing experimental data prompted the Model Basin to test machined shells which more closely fulfilled the assumptions of classical theory.[3,7,8] These tests demonstrated the effects of initial departures from sphericity together with the normally less serious effects of variations in thickness, residual stresses, and adverse boundary conditions. The collapse strength of these shells was about two to four times greater than the collapse strength of the shells formed from flat plates. By achieving a maximum 0.9 ratio of experimental collapse pressure to the classical elastic buckling pressure, these tests lend considerable support to the validity of Zoelly's small deflection theory for initially perfect spheres.

The general effect of initial imperfection or unevenness factors on the elastic buckling coefficient obtained in recent Model Basin tests of

deep spherical shells is discussed in Reference 8 and shown graphically in Figure 1. Figure 1 illustrates that no single buckling coefficient may be used in Equation [1] to calculate the strength of spherical shells which have varying degrees of initial imperfections. This figure also indicates that although the classical buckling load coefficient is apparently valid for perfect spheres, it is impossible to manufacture or measure most spherical shells with sufficient accuracy to justify the use of the classical equation in design.

Based on these recent test results, an empirical equation for near-perfect spheres was suggested which predicts collapse to occur at about 0.7 times the classical pressure. This empirical equation for the elastic buckling pressure p_3 of near-perfect spheres may be expressed as

$$p_3 = \frac{1.4\ E(h/R_o)^2}{\sqrt{3\ (1 - \upsilon^2)}} = 0.84\ E(h/R_o)^2 \text{ for } \upsilon = 0.3 \qquad [2]$$

where the use of the outer radius R_o is dictated by simple load equilibrium. Initially perfect shells may buckle at pressures approaching 43 percent greater than the pressure given by Equation [2].

The inelastic buckling strength of initially perfect spheres was first investigated by Bijlaard.[9] He obtained a plasticity reduction factor which he applied to the classical elastic buckling equation. His collapse pressure p_B may be expressed as

$$p_B = 2\sqrt{\frac{E_s E_t}{3(1 - \upsilon_p^2)}}\left(\frac{h}{R}\right)^2 = 1.34\sqrt{E_s E_t}\ (h/R)^2 \text{ for } \upsilon_p = 0.5 \qquad [3]$$

where E_s is the secant modulus,
E_t is the tangent modulus, and
υ_p is Poisson's ratio in the plastic range.

Machined deep spherical shells with ideal boundaries which collapsed at stress levels above the elastic limit of the material have also been tested at the Model Basin.[3,7] For each model tested, Bijlaard's inelastic

buckling theory (Equation [3]) gave collapse pressures higher than the corresponding experimental collapse pressures. The collapse strength of those models which failed at stress levels above the proportional limit were accurately calculated, however, using an empirical formula based on applying a plasticity reduction factor similar to Bijlaard's to the empirical Equation [2]. This empirical formula for the inelastic collapse pressure of near-perfect spheres may be expressed as

$$p_E = 1.4 \sqrt{\frac{E_s E_t}{3(1 - \nu^2)}} \left(h/R_o\right)^2 = 0.84 \sqrt{E_s E_t} \left(h/R_o\right)^2 \text{ for } \nu = 0.3 \qquad [4]$$

The secant and tangent modulus used in Equations [3], [4], and [5] are derived from typical stress-strain curves of the material obtained from simple compression specimens. In Equation [3], it is assumed on the basis of tnin-shell theory that the stress σ_1 may be calculated by

$$\sigma_1 = \frac{p\,R}{2\,h} \qquad [5]$$

In Equation [4], the average stress σ_{AVG} which satisfies equilibrium conditions for all thicknesses is used and may be calculated by

$$\sigma_{AVG} = \frac{p\,R_o^2}{2\,R\,h} \qquad [6]$$

It should be pointed out that Equation [4] neglects the change in Poisson's ratio when going from the elastic range to the plastic range. This assumption is conservative.

How well empirical Equation [4] works is demonstrated in Figure 2. The ordinate is the ratio of the experimental collapse pressure to the classical elastic buckling pressure. The abscissa is the ratio of the empirical inelastic collapse pressure to the classical buckling pressure. Both the experimental elastic and inelastic buckling pressures recorded in References 3, 7, and 8 are plotted in Figure 2 since Equation [4]

reduces to Equation [2] in the elastic range. It is apparent that Equation [4] adequately predicted the behavior of the machined models.

Since the recent tests show that the discrepancy between the early experiments and classical small deflection theory can be attributed to the failure of the experiment to fulfill the rigid theoretical assumptions, it appears worthwhile to study the effects of imperfections, or unevenness factors, on both elastic and inelastic behavior. Since most contributions to the unevenness factor, such as variations in thickness, residual stresses, boundary conditions, etc. may be, at least on occasions, fairly well controlled, the effects of initial departures from sphericity seem most worthy of investigation.

Until very recently, no theoretical or experimental work had been done to study the effects of imperfections on the strength of spherical shells. Thompson[5] and Wedellsborg[6] have recently developed analyses for the elastic buckling of initially imperfect spheres. Based on a middle surface imperfection of assumed shape and amplitude, Thompson solved the nonlinear equation for the maximum buckling pressure. This type of theoretical approach shows promise of producing the first valid theoretical elastic analysis for practical spheres and appears worthy of further investigation. Wedellsborg proposed that the elastic buckling strength of imperfect spheres could be calculated on the basis of local curvature. However, it appears that his analysis would be extremely conservative for local "dents" and unsafe for large flat spots. No theoretical work has been conducted on the inelastic buckling strength of initially imperfect shells. Prior to the current Model Basin program, no valid experimental work has been conducted on initially imperfect deep spherical shells due to insufficient measurements of initial contours.

ANALYSIS

The strength analysis for initially imperfect spherical shells with ideal boundaries presented herein is based on observations of earlier tests of machined models conducted at the Model Basin.[3,7,8,10] First, an empirical analysis was developed for both the elastic and inelastic collapse strength of near-perfect spherical shells with ideal boundaries; see Equations [2], [4], and [6]. Then tests were conducted to determine

the relationship between unsupported arc length and the elastic and inelastic collapse strength of machined shallow spherical caps with clamped edges.[3,10] The test results of the spherical caps suggested an approach to the strength analysis of initially imperfect spheres which, in essence, modifies the analysis for near-perfect spheres.

The results of the spherical segment models which failed in the elastic range are compared in Figure 3 with test results recorded in the literature[4,11-13] and with nonlinear symmetric and nonsymmetric theory.[14-18*] The ordinate is the ratio of the experimental collapse pressure to the classical pressure, and the abscissa is the nondimensional parameter θ defined as

$$\theta = \left[3/4\ (1 - \upsilon^2)\right]^{1/4} \frac{L_a}{\sqrt{Rh}} = \frac{0.91\ L_a}{\sqrt{Rh}} \text{ for } \upsilon = 0.3 \qquad [7]$$

where L_a is the unsupported arc length of the shell.

Whereas previous experiments recorded in the literature showed a complete lack of repeatability, the machined segment results followed a very definite pattern. Since the primary difference between these and earlier specimens was the magnitude of initial departures from sphericity, these results demonstrated the detrimental effects of deviations from perfect sphericity. These results also demonstrated that a short clamped segment can be weaker than a longer clamped segment. Although this phenomenon has been implied by existing theoretical studies, it found no support in the earlier experiment. It is interesting to note that for the first time there is good agreement between experiment and theory throughout the range of shallow spherical shells.

The results of the spherical segment model which failed at stress levels above the proportional limit of the material $\sigma_{P.L.}$ are presented in Figure 4. The coordinates are the same as those in Figure 3 except the empirical inelastic collapse pressure has been substituted for the

---

*In private correspondence, the authors were informed by H. Weinitschke of a programming error in his results reported in Reference 18. The corrected results obtained by Weinitschke are shown in Figure 3.

classical elastic pressure in the ordinate. The results are plotted in families of curves which basically represent varying degrees of stability; shells with the lowest P_E/P_1 are the most stable. The results demonstrate that for θ values greater than approximately 2.2, the detrimental effect of clamping the edges diminishes as the shells become more stable. Although the test results discussed thus far have been for near-perfect models, they provide the basis for the following analysis of deep spherical shells with initial imperfections.

A rather abstract assumption may be made concerning the effects of initial imperfections on the basis of the results shown in Figure 4. None of the collapse pressures for the shells associated with values of greater than about 2.2 to 2.5 were appreciably greater than that predicted for complete spheres of the same material and the same thickness to radius ratio. In slightly different terminology, clamping the edges of the spherical segments associated with θ values of 2.2 or greater did not increase their collapse strength. In fact, those shells associated with θ values in the region of 4.5 were weakened by clamping the boundary. Thus, Figure 4 demonstrates that the collapse of a spherical shell is a local phenomenon and suggests that collapse strength may be better calculated on the basis of local geometry over a critical length than on nominal geometry as has normally been used in the past. Assuming that a critical length L_c exists which may be associated with a θ value of 2.2, the expression for L_c becomes

$$L_c = \frac{2.2\sqrt{R_1 h}}{[3/4\ (1 - \nu^2)]^{1/4}} = 2.42\sqrt{R_1\ h_a} \text{ for } \nu = 0.3 \qquad [8]$$

where h_a is the average thickness over a critical length and R_1 is the local radius to the midsurface of the shell over a critical arc length associated with a θ value of 2.2.

Equations [1], [2], [4], and [6] may be readily expressed in terms of local geometry by

$$p_1' = 1.21\ E \left(h_a/R_1\right)_0^2 \qquad [9]$$

$$p_3' = 0.84\ E\left(h_a/R_{1_0}\right)^2 \qquad [10]$$

$$p_E' = 0.84\ \sqrt{E_s\ E_t}\left(h_a/R_{1_0}\right)^2 \qquad [11]$$

$$\sigma'_{AVG} = \frac{p\left(R_{1_0}\right)^2}{2\ R_1\ h_a} \qquad [12]$$

where R_{1_0} is the local radius to the outside surface of the shell over a critical arc length associated with a θ value of 2.2.

The primes in Equations [9] through [12] simply indicate that the local geometry is used to calculate the pressures and stresses. Equations [11] and [12] may be used to calculate the collapse strength of initially imperfect spheres which collapse in either the elastic or inelastic region since Equation [11] reduces to Equation [10] in the elastic region.

Since Equations [9] through [12] do not consider the effects of secondary moments, Equation [12] can be expected to predict the membrane stress at the center of a "flat spot." The consequence of not considering secondary moments will be most severe in the region of low ratios of elastic to inelastic collapse strength, that is, p_3'/p_E' ratios of 1.0 to possibly 2.0. The effect of secondary moments could be empirically accounted for by adjusting the data presented in Figure 4 to reflect the rigidity of the boundary conditions. However, it does not appear practical to do this for typical shells since it is difficult, if not impossible, to accurately describe the boundary condition supporting the local imperfections of critical length.

The above analysis assumes the absence of residual stresses, mismatch, and adverse boundary conditions and penetrations. It also assumes that the shell is loaded by only hydrostatic pressure and not by additional local static loads or dynamic loads of any kind.

Equations [10] through [12] are essentially "engineering type" solutions and are not presented as a theoretical treatment of the strength

of imperfect spherical shells. In this regard, it is highly desirable to develop a means by which the analysis may be readily applied to the design and evaluation of practical structures. The basic problem in applying the analysis is that it is necessary to determine the local radius over a critical arc length. One of the simplest ways to do this is to express the local radius in terms of deviations from a nominal radius or in terms of out-of-roundness. Figure 5 shows the assumed relationship between deviations from the nominal radius δ, out-of-roundness Δ, and local radius over a critical arc length for a Poisson's ratio of 0.3. By simple geometric relationships it can be shown that

$$\Delta/h_a = \frac{\Delta/R}{h_a/R} = \frac{(1 - \cos\phi) - R_1/R\ (1 - \cos\ \alpha)}{h_a/R} \qquad [13]$$

By assuming values for R, h_a, and $R_{1/R}$, α may be calculated by

$$\alpha = \frac{L_a/2}{R_1} = 1.21\sqrt{h_a/R_1} \qquad [14]$$

and ϕ may be calculated by

$$\cos\phi = \left[1 - \left(R_1/R\right)^2 \left(1 - \cos^2\ \alpha\right)\right]^{1/2} \qquad [15]$$

The results of Equation [13] are presented graphically in Figure 6 for two rather extreme values of h_a/R. Very significant increases in local radius are obtained for relatively small deviations from perfect sphericity. For example, the local radius is almost 1.7 times the nominal radius for a Δ/h_a of 0.5.

The effect of initial deviations from sphericity is extremely important in the elastic buckling case since the local radius appears in the appropriate equation to the second power; see Equation [10]. To demonstrate this effect in more familiar terminology, the elastic buckling coefficient K for ν of 0.3 is plotted against Δ/h_a in Figure 7. Here Equation [10] may be rewritten in terms of nominal radius as

$$p_3' = K\,E\left(h_a/R_0\right)^2 \qquad [16]$$

Considering the effect of initial imperfections is also very important when calculating the inelastic buckling strength where the collapse pressure is primarily a function of the average stress level. The average stress is approximately proportional to the local radius; see Equations [11] and [12].

It should be remembered that Δ is associated with a critical arc length which may be calculated using Equation [8]. In practice, it is often desirable to define the critical length in terms of critical chord length L_{cc}. The ratio of L_{cc}/R may be easily obtained for various values of Δ/h_a and $h_{a/R}$ by use of the graph presented in Figure 8.

EXPERIMENT

DESCRIPTION OF MODELS

The three series of models were designed to study the effect of local imperfections on the hydrostatic collapse strength of deep spherical shells and consisted of the following:

1. Series FS consisted of 36 models of hemispherical shells each bounded by a ring-stiffened cylinder designed to provide conditions of membrane deflection and no rotation to the edge of the hemisphere. A local flat spot was present in the apex of each hemisphere.

2. Series VT consisted of 12 models of hemispherical shells each bounded by membrane cylinders. A local thin spot was present in the apex of each hemisphere.

3. Series ET consisted of 14 models of spherical segments which clamped edges. A local thin spot was present in the apex of each segment.

Series FS and VT were designed to study both the elastic and inelastic buckling strength of initially imperfect spherical shells. Thus, the ratios of shell thickness to radius were selected to study relatively stable as well as unstable configurations. Series ET was designed to study only the elastic buckling strength of spherical shells with local thin spots.

All models in each series were machined from 7075-T6 aluminum bar stock with a nominal yield strength of 80,000 psi. Young's modulus E for the material, as determined by optical strain gage measurements, was 10.8×10^6 psi. A Poisson's ratio ν of 0.3 in the elastic range was assumed. Tables 1-3 give the model dimensions for each series, and Figure 9 shows representative ratios of $[E_s E_t]^{1/2}$ to E as a function of uniaxial compressive stress for the material used in each model.

Series FS Models

Series FS consisted of 36 machined models of hemispherical shells with local flat spots. The flat spots, which were machined in the apex of each model, had an included angle of 10 deg for Models FS-1 through FS-9, 20 deg for Models FS-10 through FS-27, and 30 deg for Models FS-28 through FS-36. The local radius of curvature was held constant for each flat spot and was 1.15 times the nominal radius for Models FS-10 through FS-18 and 1.4 times the nominal radius for all remaining models.

Each model was machined in an identical manner. The interior contours were machined by use of form tools, the exterior contours by supporting the inside contours on a mating mandrel and by generating the outside surface using a lathe with a ball-turning attachment.

The wall thickness of each model was measured using a small support-ball and a dial gage. The total variation in measured wall thickness was normally less than 1 percent of the shell thickness. The flat spot contours were checked by comparing measured deviations from sphericity at the center of the flat spots with calculated values. Excellent agreement was obtained for each model.

Series VT Models

Series VT consisted of 12 machined models of hemispherical shells with local thin spots at the apex. The models were machined in a manner identical to that used for Series FS. The thin spots were obtained by removing material on the exterior surfaces and had chord lengths from about 0.17 to 1.0 times the radius.

The wall thickness of each model was measured at the apex and at the edge of the thin spot by use of a support-ball and a dial gage. Unfortunately, the initial contours were not measured.

Series ET Models

Series ET consisted of 14 machined models of spherical segments with local thin spots at the apex. The arc length of the segments was of sufficient length to disregard the effect of the clamped edges.[3] The thickness to radius ratio was selected to ensure collapse in the elastic region. The interior contours were generated using a specially designed tool.[8] The exterior contours were obtained by supporting the inside contours by a mating mandrel and by generating the outside surface using a lathe with a ball-turning attachment.

The variation in local inside radii was measured by pivoting a dial gage clamped to the special tool for generating inside spherical surfaces. Representative measurements are shown in Table 3. These measurements indicate that the interior contours deviated from perfect sphericity and suggest that some residual stresses were present in the models.*

TEST PROCEDURE AND RESULTS

Each model was tested under external hydrostatic pressure. Pressure was applied in increments and each new pressure level was held at least 1 minute. The final pressure increment was always less than 2 percent of the maximum pressure. Every effort was made to mimimize any pressure surge when applying pressure.

Tables 4-6 present the experimental collapse pressures. Photographs of representative models after collapse are shown in Figure 10.

COMPARISON OF ANALYSIS WITH EXPERIMENT

Figure 11 compares the experimental results with the analysis developed in this report. The ordinate is the ratio of the experimental collapse pressure to the modified classical pressure p_1' as presented in Equation [9]. The abscissa is the ratio of the empirical inelastic buckling pressure p_E' to p_1'. The abscissa, therefore, is a measure of the stability of a spherical shell, i.e., the lower values of p_E'/p_1' are the most stable.

---

*The models could not be stress relieved since 7075-T6 aluminum loses its strength when subjected to temperatures sufficient for stress relieving.

The comparison between experiment and theory is good, particularly for the more stable shells. The scatter shown for the less stable shells requires a closer examination of geometries involved.

The experimental results of the flat spot series models are compared with the imperfection analysis is presented in Figure 12. The abscissa is the nondimensional parameter β defined as

$$\beta = [3/4\ (1 - \nu^2)]^{1/4} \frac{L_i}{\sqrt{R_L\ h_{MIN}}} \qquad [17]$$

where L_i is the midsurface arc length of the imperfection,

R_L is the radius of the midsurface of the imperfection, and

h_{MIN} is the minimum measured thickness of the imperfection.

The ordinate is the ratio of the experimental collapse pressure to the pressure predicted by Equation [11]. The thickness h_a was the measured thickness at the center of the flat spot. For those models with β values greater than 2.2, R_{1_0} is equal to $R_2 + h_a$ (see Table 1 and comments on measurements after fabrication). For those models with β values less than 2.2, R_1 was determined by passing a radius through a point on the midsurface of the boundary spherical shell and through the point at the midsurface at the center of the flat spot, over an arc length associated with a θ value of 2.2. Model results are presented in terms of margins of stability. Those models with ratios R_2/R_I of 1.15 are marked with an asterisk. All other models had R_2/R_I ratios of 1.40.

For the wide range of β values investigated, Figure 12 indicates that the comparison between experiment and analysis is good. With the exception of eight model tests, all of the models collapsed at pressures within approximately 10 percent of predictions. Two things characterize those model results which fall more than 10 percent below the predicted pressures. All of these models had margins of stability of less than 1.2 and ratios R_2/R_I of 1.40. Figure 4 indicates that secondary moments, which

are not considered in the imperfection analysis, have a significant effect on the collapse strength of the less stable shells. As indicated in Table 1, the flat spot models had abrupt changes in curvature. This would not be true for imperfections in most practical shells. Thus the flat spots investigated by this series of models were severe. Another significant result of the flat spot series tests is that the collapse strength of all models with Δ values less than approximately 5 percent of the thickness could be predicted by Equation [2]. Thus, the collapse strength of spherical shells whose out-of-roundness Δ is less than about 2 to 3 percent of the shell thickness and whose strength is not affected by residual stresses, variations in thickness, adverse boundary conditions or other factors may be adequately calculated by the empirical formula developed for near-perfect spheres.

The results of the ET series and VT series tests are plotted in Figure 13. The abscissa is the nondimensional parameter β as defined by Equation [17]. Again the ordinate is the ratio of the experimental collapse pressure to that predicted by Equation [11]. For those models with β values greater than 2.2, R_{l_0} was determined from the point at the midsurface at the center of the thin spot to a point at the midsurface located at a distance $L_c/2$ from the center. For the ET series models, measurements made after fabrication were taken into consideration in the determination of R_{l_0}. For the VT-series, nominal model dimensions were used (see comments under Description of Models). The thickness h_a was the average of the thicknesses at these two points. The same procedure was followed in determining R_{l_0} and h_a for those models with θ values less than 2.2. The thickness h_a for this case was the average of the thickness at the center of the thin spot and the thickness of the boundary spherical shell. Thus, in all cases, the determination of the critical local geometry was made over an arc length associated with the critical value of θ.

Considering the severity of the imperfections machined in these models, the agreement between the analysis and experiment is quite good. Thicknesses at the center of the thin spots ranged from approximately 50 to 80 percent of the thickness at the edge, and all of the material removed for the thin spot was taken from one side of the shell, causing significant changes in curvature. In practice, thin spots would be much less severe.

In addition, most of the models had relatively low margins of stability. As indicated in Figure 13, only one model failed at a pressure more than 10 percent below that predicted by the analysis. Many of the models failed well above predictions. The collapse of those models with β values greater than approximately five were influenced by the nonsymmetric mode of failure. Whereas thicknesses were averaged over the center portion of these thin spots, the models failed in the nonsymmetric mode at the boundary where thicknesses were significantly greater; see Figure 10, Model ET-13.

Residual stresses were present in the ET series as demonstrated by their failure to hold their contour during the last stages of the machining process. Since measurements were not taken on the VT series models, it is possible that residual stresses were present. It is difficult if not impossible to determine the effects of residual stresses on the observed collapse pressures.

Several important factors are not as yet considered by the imperfection analysis presented in this report. The analysis does not consider the effects of secondary moments or adverse boundary conditions. The importance of these effects has been mentioned in discussing the model results and is shown in Figure 4. For relatively unstable shells, the reduction in collapse strength due to adverse boundary conditions is significant. As the shells become more stable, however, these effects diminish. Another factor not considered by the analysis is the effect of residual stresses on collapse strength. It would be extremely difficult to take into account theoretically the residual stresses in a shell fabricated according to practical large-scale procedures since the residual stresses would be present in the shell in some random, unpredictable pattern. The best approach to this problem appears to be empirical. The Model Basin has conducted an experimental parametric study of large pressed and welded hemispheres in the fabricated and in the stress-relieved condition. The elastic behavior of these hemispheres agrees well with the imperfection analysis reported here. The collapse pressures achieved for the as-fabricated and stress-relieved shells follow very definite patterns when the imperfection analysis is applied. A report on the results of these tests is in preparation.

Because of the urgent need for rational design criteria for spherical shells, the results reported to date have had an empirical bias. Additional programs which include theoretical as well as experimental treatments are currently being conducted at the Model Basin under the sponsorship of the Bureau of Ships. The effects of flat spots, boundary conditions, mismatch, penetrations, stiffening systems, residual stresses, and laminated construction on the elastic behavior and collapse strength of spherical shells are being studied. Parametric model studies of practical shells of new materials are also being conducted. It remains clear that the presence of initial imperfections must be considered in the formulation of any large deflection analysis before such analysis can be expected to quantitatively predict the collapse strength of practical spherical shells.

The imperfection analysis presented in this report has been verified by the results obtained to date from these studies. Briefly, the analysis involves the determination of the critical local geometry of a spherical shell over an arc length associated with a θ value of 2.2 and the use of this geometry and not nominal geometry in Equations [11] and [12]. In analyzing a practical spherical shell, this requires an accurate determination of the contours of the shell. Local radii may be determined from these contour measurements with the aid of Figure 6. Thickness measurements must then be taken and correlated with the contour measurements to determine the critical value of h_a/R_{l_0}. From the design standpoint, a minimum thickness must be assumed and acceptable tolerances on shape must consider realistic fabrication techniques and the effects of out-of-roundness on strength.

CONCLUSIONS

1. Equation [11] may be used to adequately calculate the effects of initial departure from sphericity and thickness variations on elastic and inelastic collapse strength.

2. The collapse of spherical shells is primarily a local phenomenon and is therefore critically dependent on local geometry.

3. Equation [4] may be used to adequately calculate the collapse strength of near-perfect spherical shells whose out-of-roundness Δ is less than about 2 to 3 percent of a shell thickness and whose strength is not affected by residual stresses, variations in thickness, adverse boundary conditions, or other factors.

4. The presence of initial imperfections must be considered in the formulation of any large deflection analysis before such analyses can be expected to quantitatively predict the collapse strength of practical spherical shells.

ACKNOWLEDGMENTS

The authors acknowledge the contributions of Mr. Hugh Davidson who was responsible for the reduction and presentation of the data and Mr. Leonard Giuffreda who conducted the hydrostatic tests.

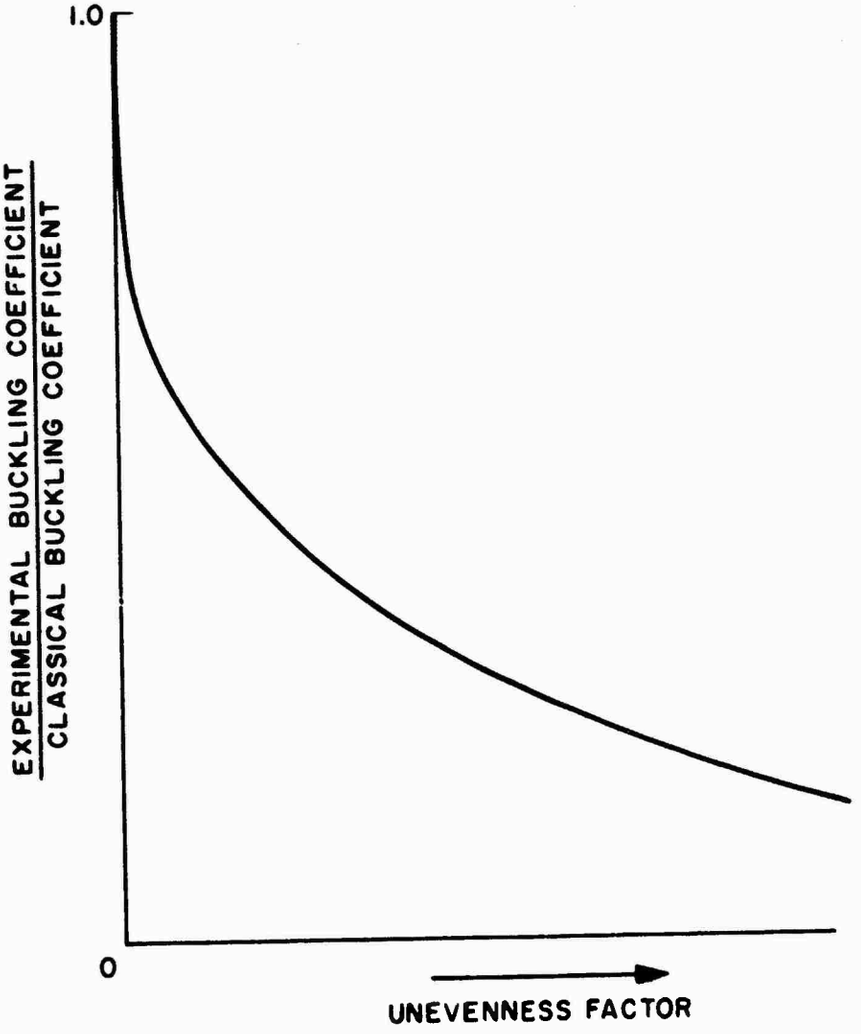

Figure 1 - Effect of Initial Imperfections on the Elastic Buckling Coefficient for Spherical Shells

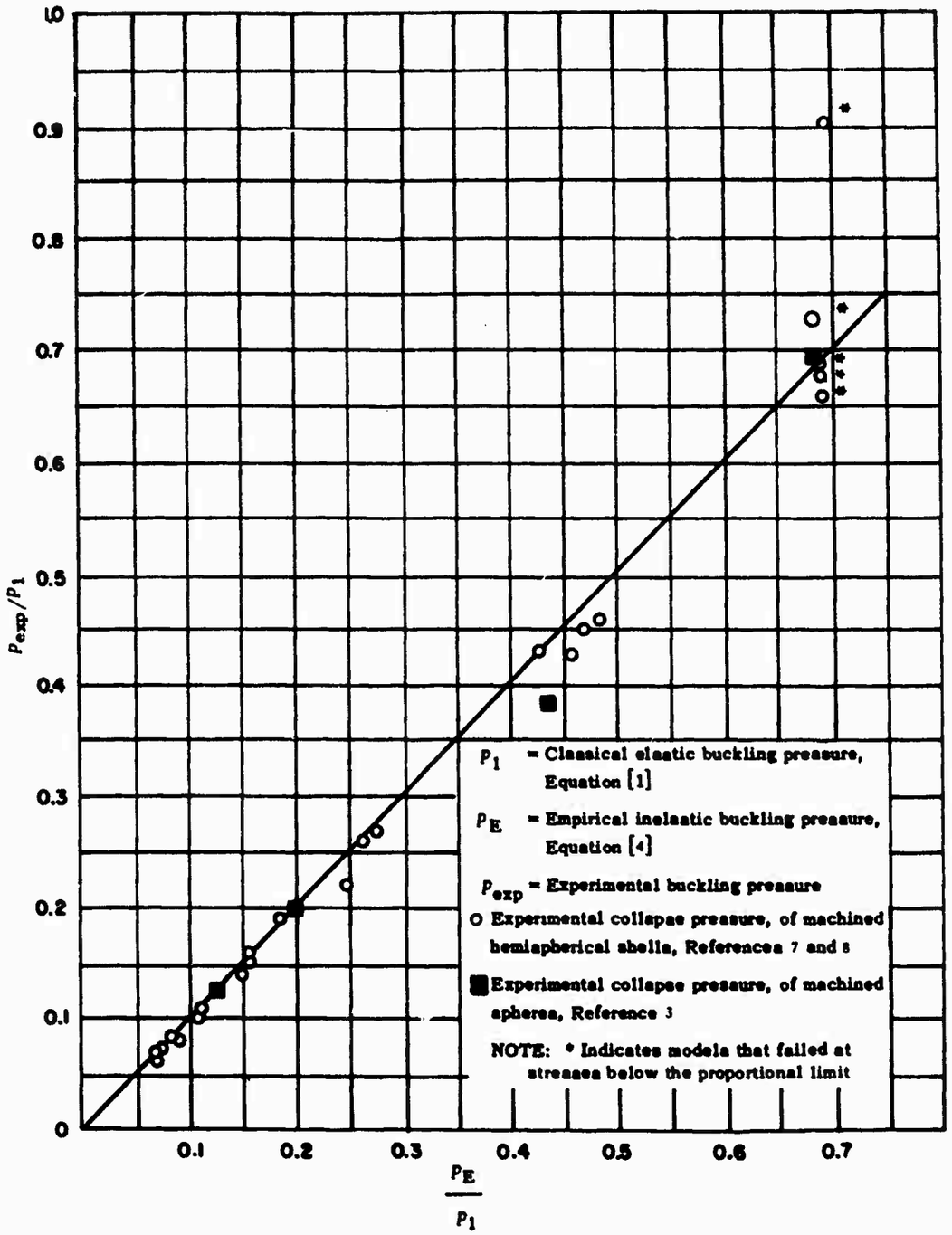

Figure 2 - Experimental Buckling Data for Near-Perfect Deep Spherical Shells with Ideal Boundaries

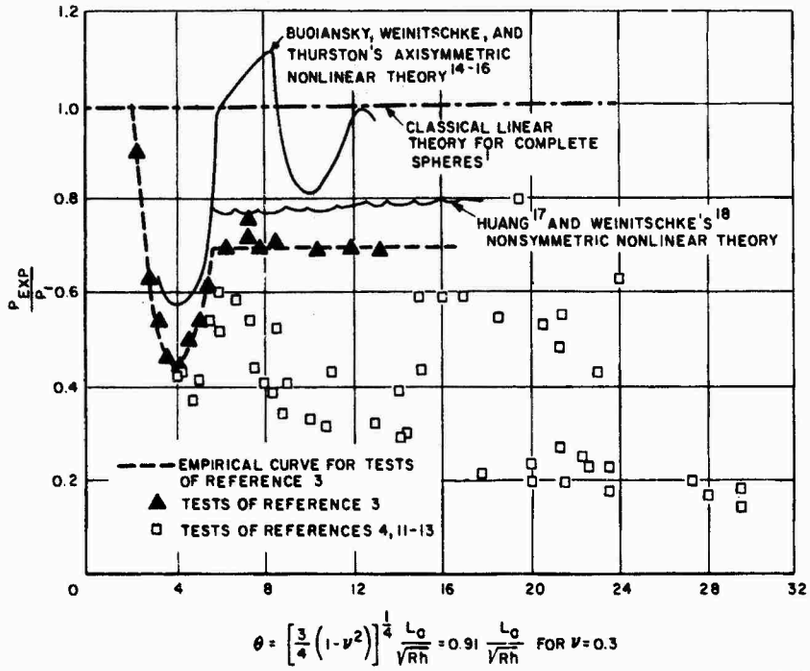

Figure 3 - Experimental Elastic Buckling Data for Shallow Spherical Shells with Clamped Edges

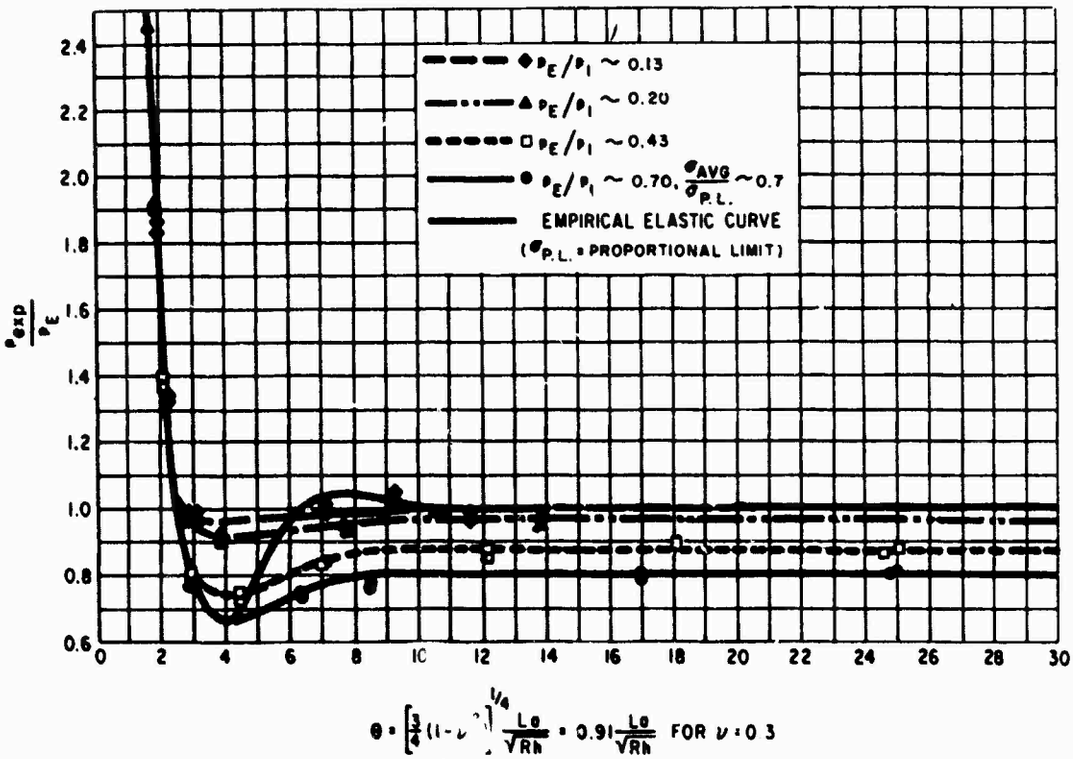

Figure 4 - Experimental Inelastic Buckling Data for Machined Shallow and Deep Spherical Shells with Clamped Edges

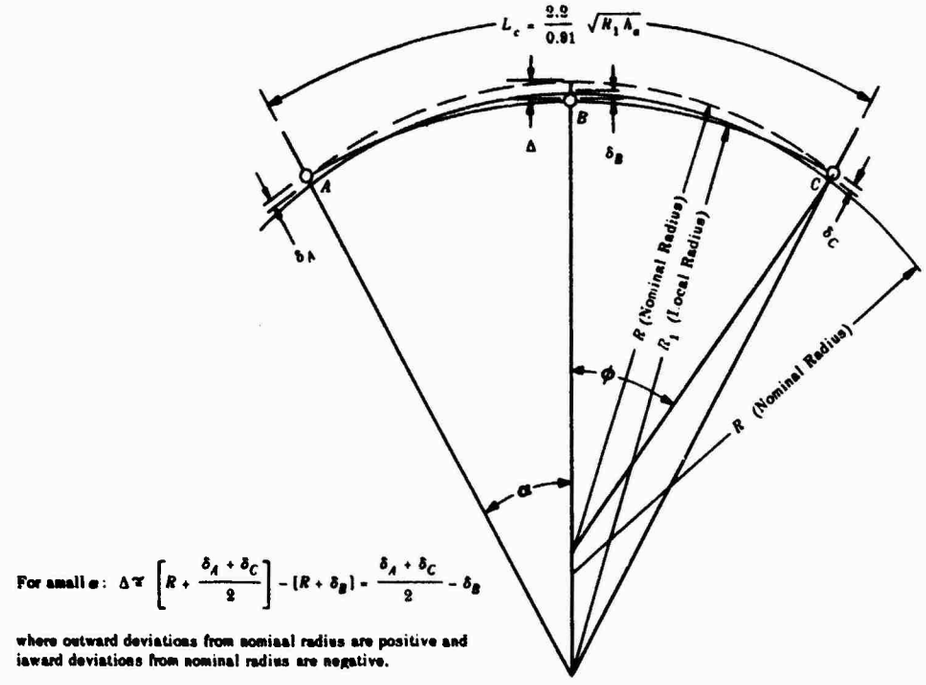

For small α: $\Delta \approx \left[R + \frac{\delta_A + \delta_C}{2}\right] - [R + \delta_B] = \frac{\delta_A + \delta_C}{2} - \delta_B$

where outward deviations from nominal radius are positive and inward deviations from nominal radius are negative.

Figure 5 - Assumed Relationship between Out-of-Roundness Δ and Local Radius R_1

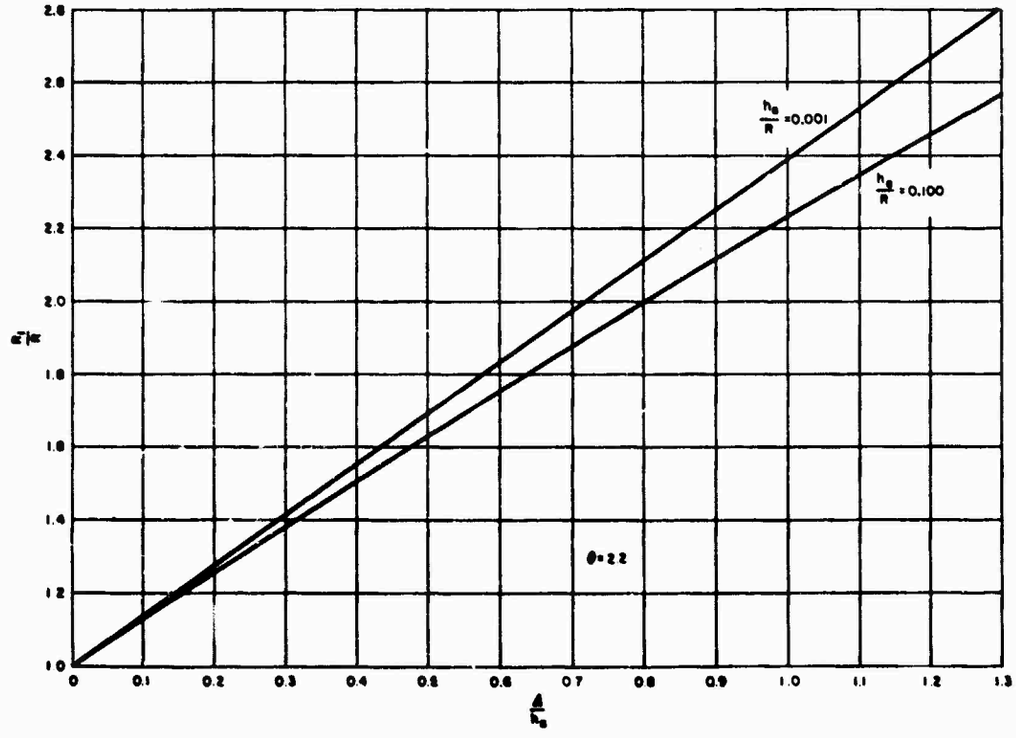

Figure 6 - Relationship between R_1/R and Δ/h_a

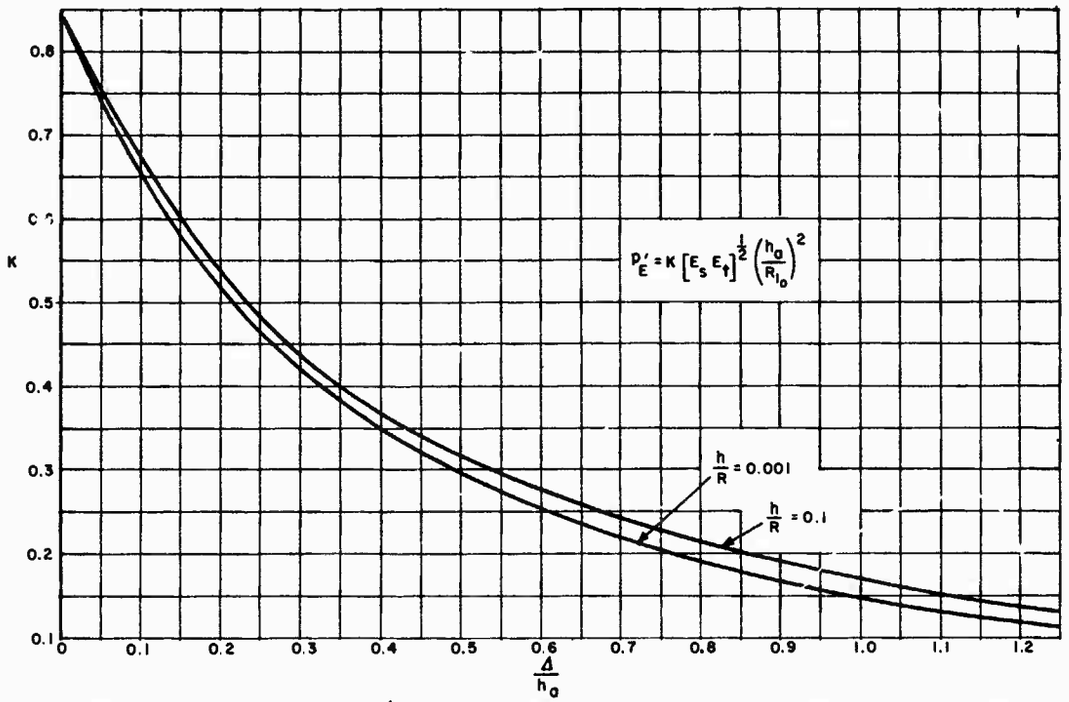

Figure 7 - Effect of Δ/h_a on the Elastic Buckling Coefficient for Spherical Shells, K

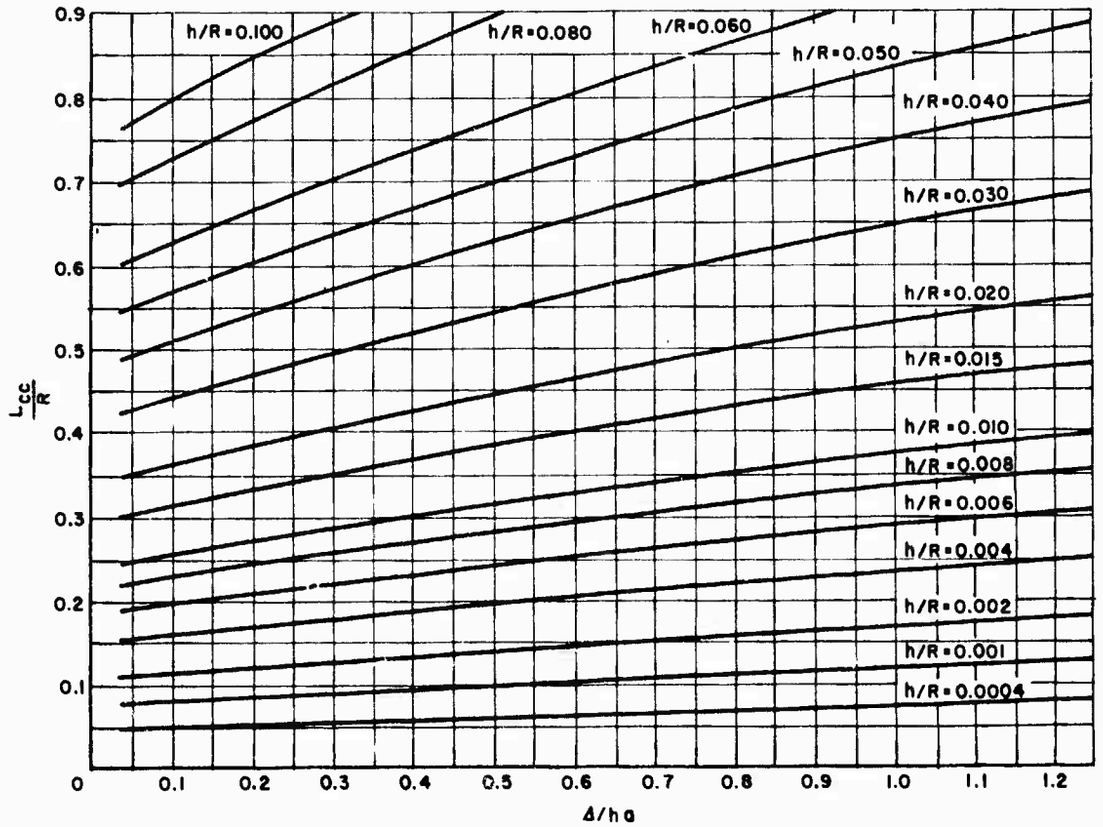

Figure 8 - Relationship between L_{cc}/R and Δ/h_a

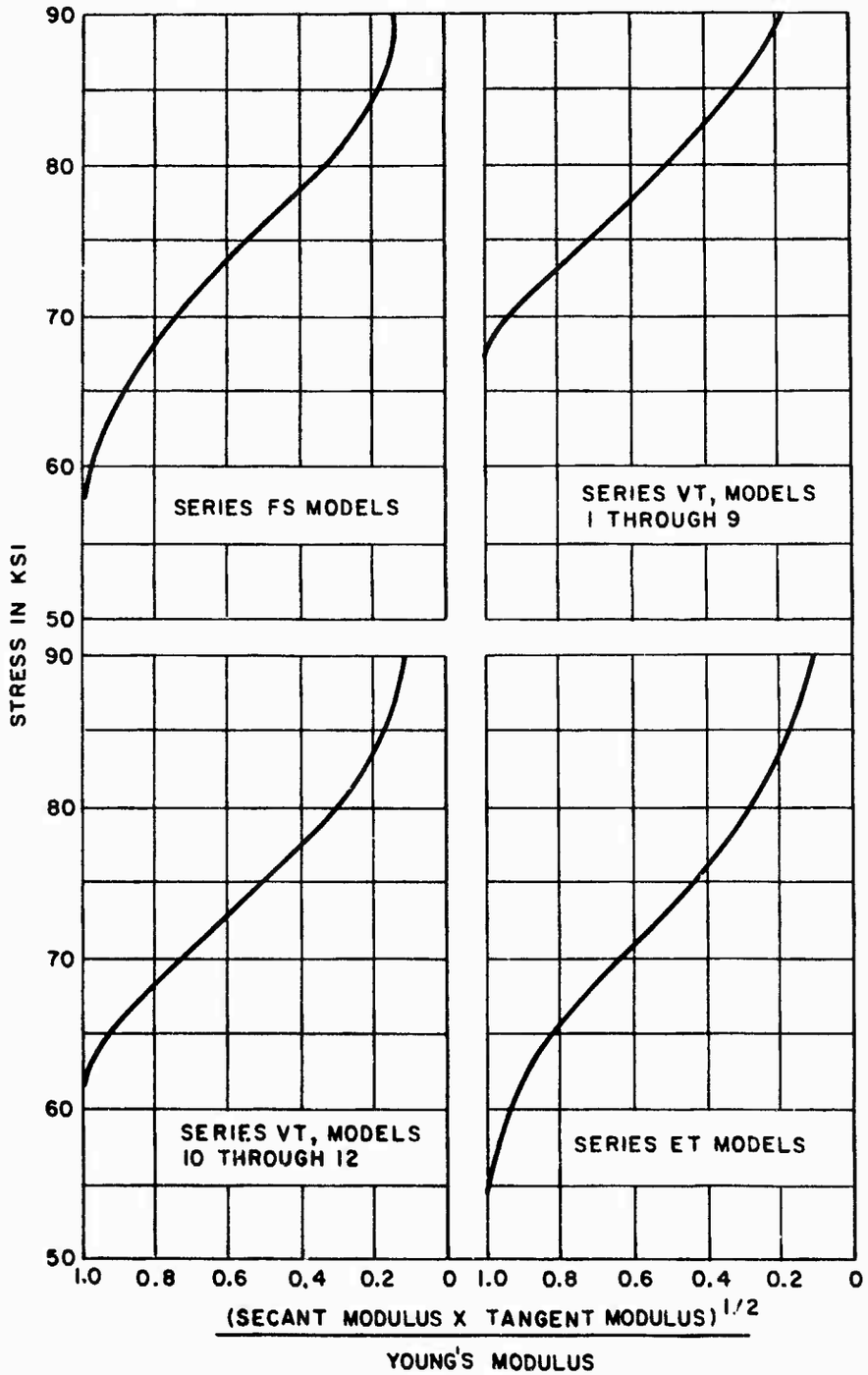

Figure 9 - Representative Material Characteristics

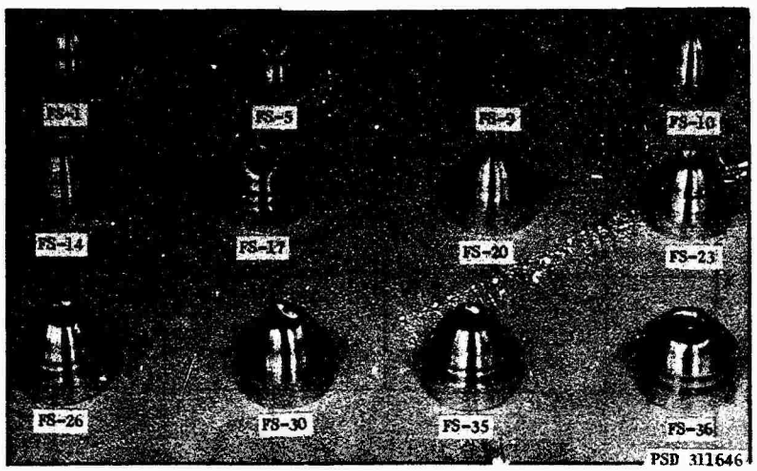

Figure 10a - Series FS

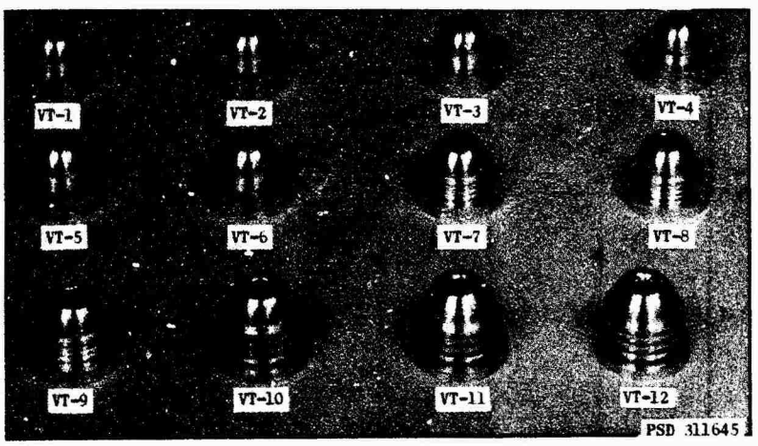

Figure 10b - Series VT

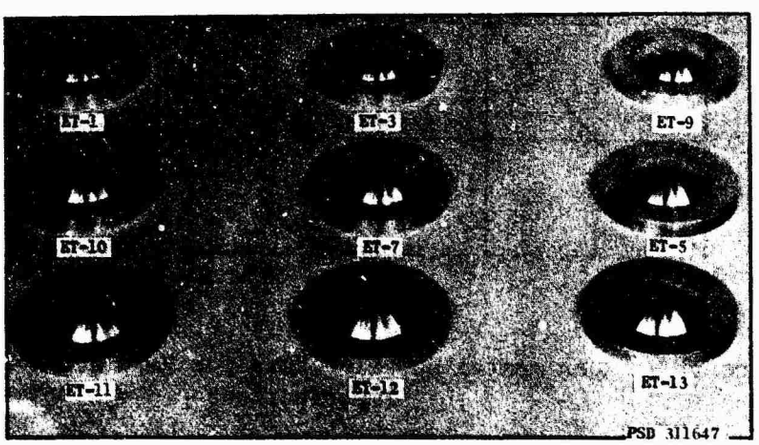

Figure 10c - Series ET

Figure 10 - Samples of Collapsed Models

612 100

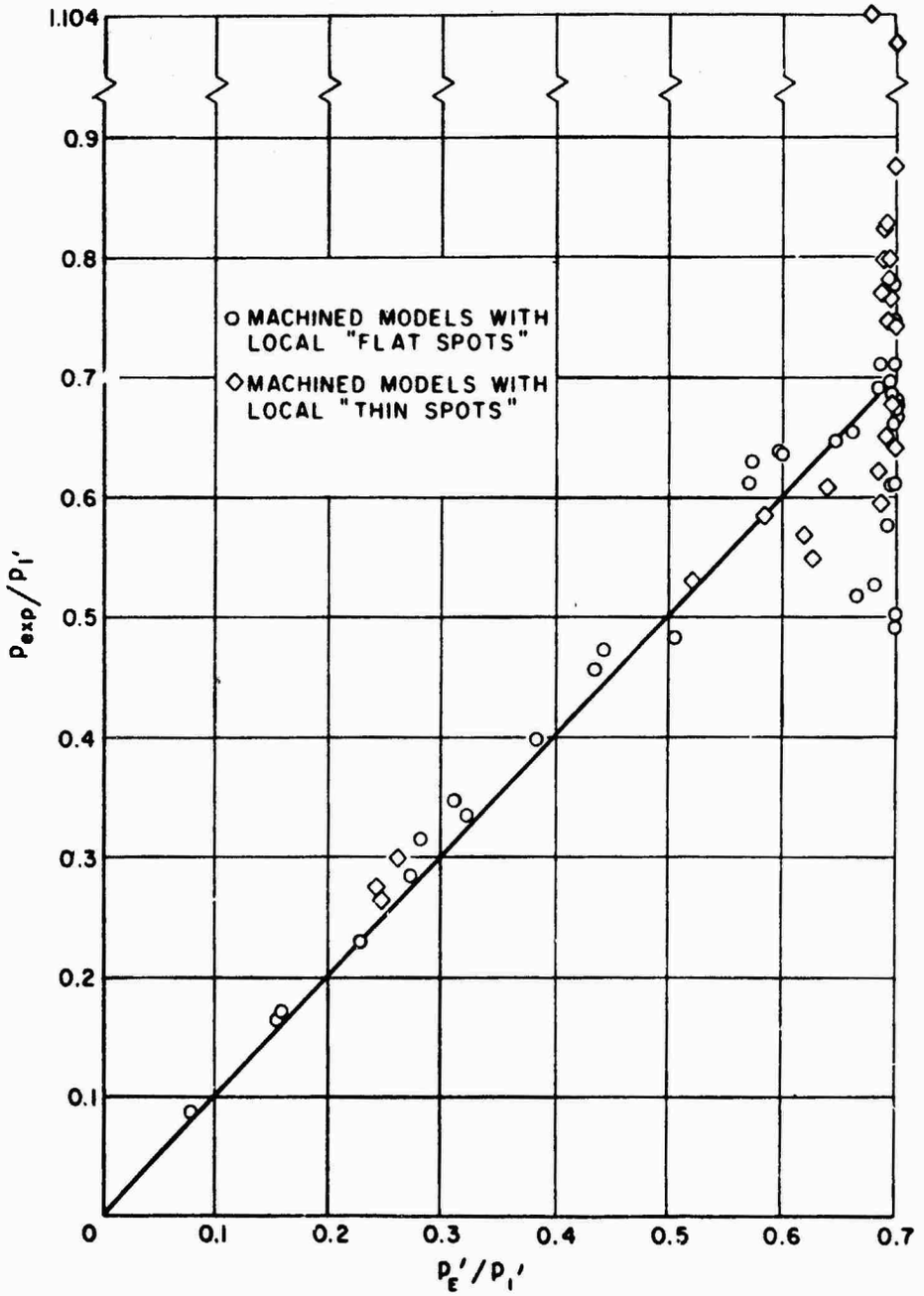

Figure 11 - Experimental Buckling Data for Machined Models with Imperfections

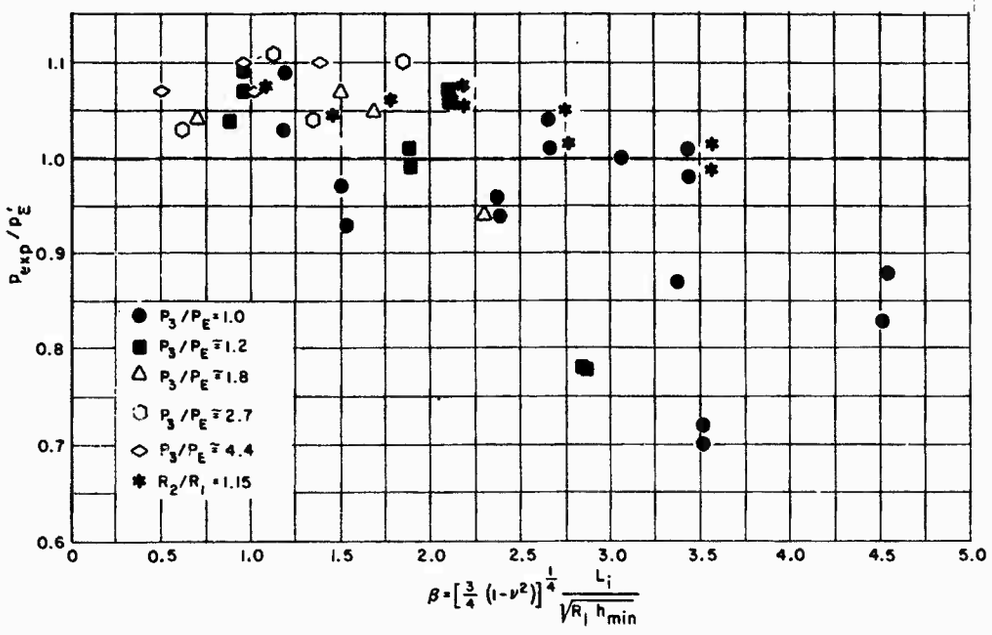

Figure 12 - Experimental Buckling Data for Series FS Models

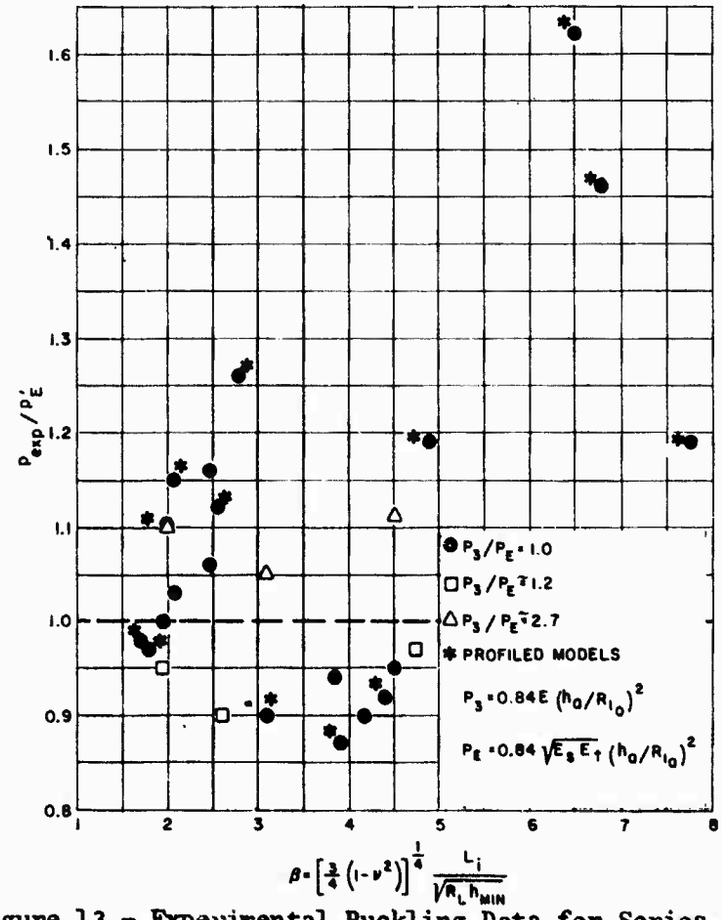

Figure 13 - Experimental Buckling Data for Series VT and Series ET Models

TABLE I

Series FS Model Dimensions

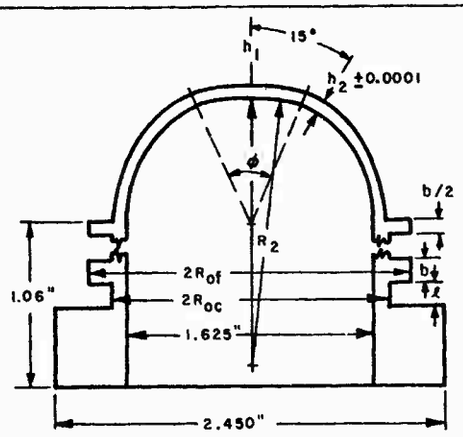

Model	h_1 in.	h_2 in.	ϕ deg.	R_2 in.	b in.	ℓ in.	$2R_{oc}$ in.	$2R_{of}$ in.	Number of "ℓ's"
FS- 1	0.0061	0.0062	10	1.138	0.022	0.044	1.638	1.688	4
FS- 2	0.0064	0.0064	10	1.138	0.022	0.044	1.638	1.688	4
FS- 3	0.0104	0.0104	10	1.138	0.028	0.055	1.648	1.702	4
FS- 4	0.0104	0.0104	10	1.138	0.028	0.055	1.648	1.702	4
FS- 5	0.0162	0.0162	10	1.138	0.079	0.079	1.661	1.751	3
FS- 6	0.0159	0.0161	10	1.138	0.079	0.079	1.661	1.751	3
FS- 7	0.0247	0.0249	10	1.138	0.090	0.090	1.683	1.827	3
FS- 8	0.0399	0.0400	10	1.138	0.115	0.115	1.717	1.967	2
FS- 9	0.0694	0.0696	10	1.138	0.154	0.154	1.789	2.338	2
FS-10	0.0062	0.0052	20	0.934	0.022	0.044	1.638	1.688	4
FS-11	0.0063	0.0063	20	0.934	0.022	0.044	1.638	1.688	4
FS-12	0.0101	0.0101	20	0.934	0.028	0.055	1.648	1.702	4
FS-13	0.0102	0.0102	20	0.934	0.028	0.055	1.648	1.702	4
FS-14	0.0159	0.0161	20	0.934	0.079	0.079	1.661	1.751	3
FS-15	0.0159	0.0160	20	0.934	0.079	0.079	1.661	1.751	3
FS-16	0.0250	0.0250	20	0.934	0.090	0.090	1.683	1.827	3
FS-17	0.0398	0.0399	20	0.934	0.115	0.115	1.717	1.967	2
FS-18	0.0694	0.0697	20	0.934	0.154	0.154	1.789	2.338	2
FS-19	0.0050	0.0051	20	1.138	0.022	0.044	1.638	1.688	4
FS-20	0.0061	0.0061	20	1.138	0.022	0.044	1.638	1.688	4
FS-21	0.0102	0.0102	20	1.138	0.028	0.055	1.648	1.702	4
FS-22	0.0104	0.0103	20	1.138	0.028	0.055	1.648	1.702	4
FS-23	0.0158	0.0160	20	1.138	0.079	0.079	1.661	1.751	3
FS-24	0.0157	0.0161	20	1.138	0.079	0.079	1.661	1.751	3
FS-25	0.0251	0.0251	20	1.138	0.090	0.090	1.683	1.827	3
FS-26	0.0400	0.0400	20	1.138	0.115	0.115	1.717	1.967	2
FS-27	0.0698	0.0699	20	1.138	0.154	0.154	1.789	2.338	2
FS-28	0.0061	0.0061	30	1.138	0.022	0.044	1.638	1.688	4
FS-29	0.0063	0.0063	30	1.138	0.022	0.044	1.638	1.688	4
FS-30	0.0104	0.0104	30	1.138	0.028	0.055	1.648	1.702	4
FS-31	0.0104	0.0104	30	1.138	0.028	0.055	1.648	1.702	4
FS-32	0.0161	0.0163	30	1.138	0.079	0.079	1.661	1.751	3
FS-33	0.0158	0.0159	30	1.138	0.079	0.079	1.661	1.751	3
FS-34	0.0248	0.0248	30	1.138	0.090	0.090	1.683	1.827	3
FS-35	0.0387	0.0387	30	1.138	0.115	0.115	1.717	1.967	2
FS-36	0.0700	0.0701	30	1.138	0.154	0.154	1.789	2.338	2

TABLE 2

Series VT Model Dimensions

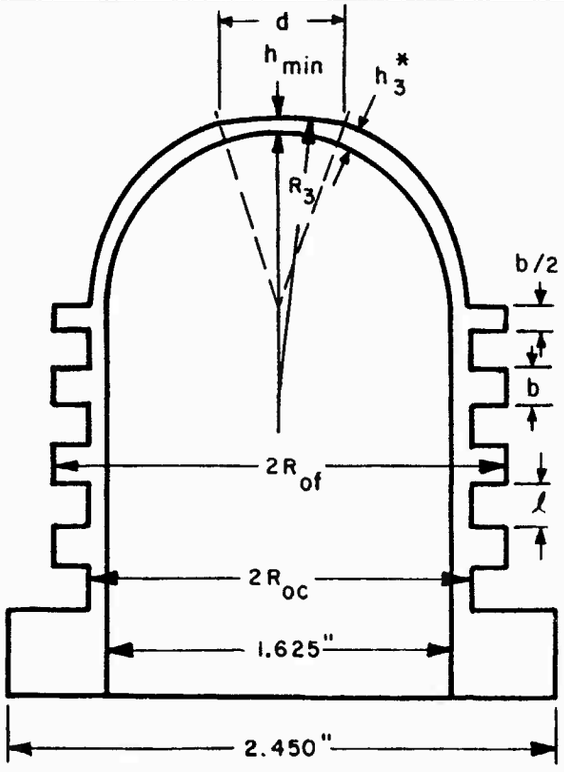

*TAKEN AT EDGE OF THIN SPOT

Model	h_{min} in.	h_3 in.	d in.	R_3 in.	b in.	ℓ in.	$2R_{oc}$ in.	$2R_{of}$ in.
VT- 1	0.0049	0.0067	0.135	1.860	0.029	0.058	1.649	1.721
VT- 2	0.0049	0.0069	0.144	1.860	0.029	0.058	1.649	1.721
VT- 3	0.0048	0.0064	0.170	1.224	0.029	0.058	1.649	1.721
VT- 4	0.0048	0.0065	0.169	1.224	0.029	0.058	1.649	1.721
VT- 5	0.0048	0.0064	0.286	0.916	0.029	0.058	1.649	1.721
VT- 6	0.0048	0.0064	0.308	0.916	0.029	0.058	1.649	1.721
VT- 7	0.0158	0.0212	0.245	1.833	0.080	0.080	1.671	1.783
VT- 8	0.0148	0.0205	0.311	1.250	0.080	0.080	1.671	1.783
VT- 9	0.0149	0.0204	0.565	0.931	0.080	0.080	1.671	1.783
VT-10	0.0386	0.0512	0.396	1.831	0.129	0.129	1.741	1.990
VT-11	0.0390	0.0517	0.599	1.294	0.129	0.129	1.741	1.990
VT-12	0.382	0.0515	0.846	0.954	0.129	0.129	1.741	1.990

TABLE 3

Series ET Model Dimensions

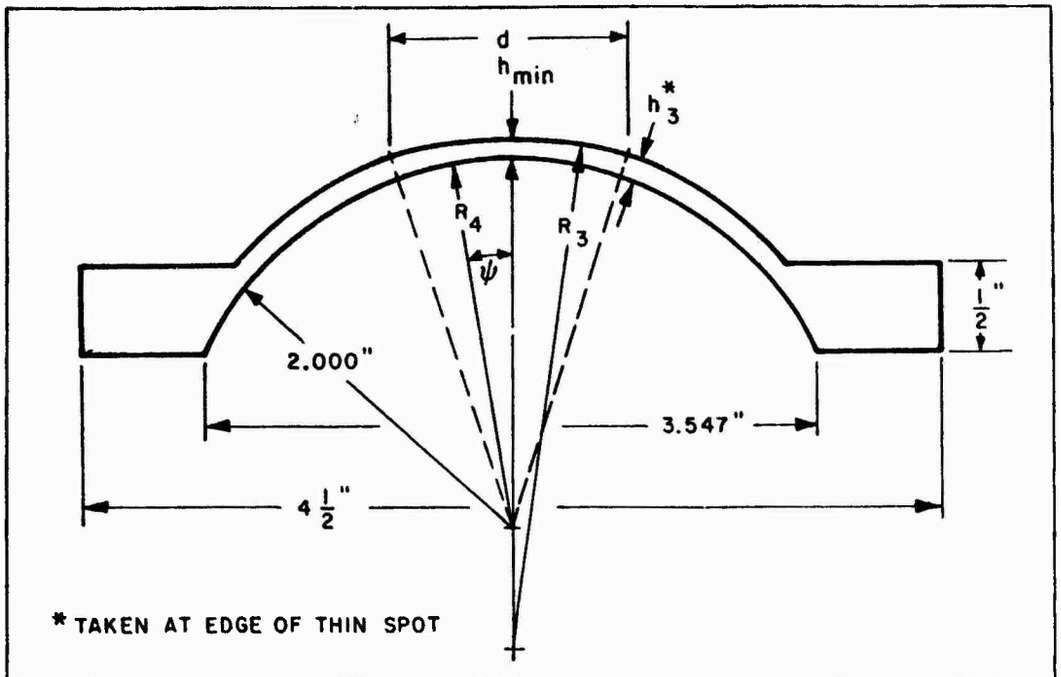

Model	h_{min} in.	h_3 in.	d in.	R_3	$\Delta R_4 = R_4 - 2.0000$			
					$\psi = 0°$	$\psi = 2°$	$\psi = 4°$	$\psi = 6°$
ET- 1	0.0087	0.0153	0.25	∞	0.0040	0.0037	0.0018	0.0011
ET- 2	0.0107	0.0158	0.29	7.87	0.0040	0.0040	0.0030	0.0025
ET- 3	0.0098	0.0155	0.30	6.02	0.0037	0.0035	0.0031	0.0028
ET- 4	0.0104	0.0157	0.33	4.68	0.0015	0.0015	0.0015	0.0015
ET- 5	0.0073	0.0155	0.37	3.66	0.0050	0.0050	0.0035	0.0027
ET- 6	0.0107	0.0158	0.41	3.17	0.0025	0.0020	0.0014	0.0010
ET- 7	0.0103	0.0156	0.49	2.69	0.0035	0.0025	0.0015	0.0010
ET- 8	0.0090	0.0135	0.57	2.47	0.0040	0.0032	0.0027	0.0022
ET- 9	0.0115	0.0159	0.65	2.35	0.0025	0.0015	0.0010	0.0008
ET-10	0.0114	0.0152	0.73	2.27	0.0034	0.0032	0.0030	0.0028
ET-11	0.0115	0.0157	0.81	2.21	0.0020	0.0020	0.0018	0.0015
ET-12	0.0085	0.0159	0.97	2.17	0.0012	0.0010	0.0006	0.0002
ET-12A	0.0085	0.0155	0.93	2.29	0.0000	0.0001	0.0002	0.0004
ET-13	0.0115	0.0158	1.29	2.09	0.0030	0.0029	0.0024	0.0010

TABLE 4

Summary of Geometric Parameters and Collapse Pressures for Series FS Models

Model	p_{exp} psi	R_{l_0} in.	h_a in.	$p_E' = 0.84\sqrt{E_s E_t}\left(h_a/R_{l_0}\right)^2$ psi	p_{exp}/p_E'	$\beta = 0.91\, L_i / \sqrt{R_L\, h_a}$
FS- 1	328	0.99	0.0061	354	0.93	1.53
FS- 2	385	0.97	0.0064	398	0.97	1.50
FS- 3	1,295	0.92	0.0104	1,190	1.09	1.18
FS- 4	1,230	0.92	0.0104	1,190	1.03	1.18
FS- 5	2,650	0.89	0.0162	2,470	1.07	0.95
FS- 6	2,625	0.89	0.0159	2,390	1.09	0.96
FS- 7	4,280	0.86	0.0247	4,125	1.09	0.77
FS- 8	7,200	0.86	0.0399	6,960	1.03	0.62
FS- 9	13,100	0.89	0.0694	12,280	1.07	0.49
FS-10	388	0.94	0.0062	397	0.98	3.45
FS-11	416	0.94	0.0063	410	1.01	3.43
FS-12	1,050	0.95	0.0101	1,013	1.04	2.66
FS-13	1,040	0.95	0.0102	1,030	1.01	2.67
FS-14	2,375	0.94	0.0159	2,235	1.06	2.11
FS-15	2,385	0.94	0.0159	2,230	1.07	2.11
FS-16	4,215	0.94	0.0250	4,025	1.05	1.68
FS-17	7,110	0.91	0.0398	6,836	1.04	1.35
FS-18	12,900	0.91	0.0694	12,110	1.07	1.02
FS-19	153	1.14	0.0050	175	0.87	3.38
FS-20	260	1.14	0.0061	260	1.00	3.06
FS-21	678	1.15	0.0102	718	0.94	2.37
FS-22	718	1.15	0.0104	747	0.96	2.35
FS-23	1,830	1.08	0.0158	1,850	0.99	1.88
FS-24	1,820	1.07	0.0157	1,810	1.01	1.89
FS-25	3,880	1.00	0.0251	3,640	1.07	1.50
FS-26	7,125	0.96	0.0400	6,410	1.11	1.22
FS-27	12,950	0.65	0.0698	11,740	1.10	0.96
FS-28	228	1.14	0.0061	260	0.88	4.59
FS-29	230	1.14	0.0063	276	0.83	4.51
FS-30	535	1.15	0.0104	747	0.72	3.52
FS-31	525	1.15	0.0104	747	0.70	3.52
FS-32	1,325	1.15	0.0161	1,700	0.78	2.84
FS-33	1,300	1.15	0.0158	1,675	0.78	2.86
FS-34	2,850	1.16	0.0248	3,025	0.94	2.30
FS-35	5,800	1.08	0.0387	5,250	1.10	1.85
FS-36	12,000	1.01	0.0700	10,950	1.10	1.41

TABLE 5

Summary of Geometric Parameters and Collapse Pressures for Series VT Models

Model	p_{exp} psi	R_{1_0} in.	h_a in.	$p'_E = 0.84\sqrt{E_s E_t}\left(h_a/R_{1_0}\right)^2$ psi	p_{exp}/p'_E	$\beta = 0.91\, L_i / \sqrt{R\, h_{min}}$
VT- 1	335	0.99	0.0058	311	1.00	1.95
VT- 2	350	1.00	0.0059	312	1.03	2.08
VT- 3	315	0.98	0.0056	298	1.06	2.48
VT- 4	345	0.99	0.0057	298	1.16	2.47
VT- 5	275	0.87	0.0053	300	0.90	4.18
VT- 6	290	0.86	0.0052	306	0.95	4.51
VT- 7	2,660	0.99	0.0185	2,665	0.95	1.96
VT- 8	2,200	1.01	0.0177	2,315	0.90	2.59
VT- 9	2,365	0.88	0.0163	2,335	0.97	4.75
VT-10	7,690	1.01	0.0449	6,815	1.10	2.03
VT-11	7,150	0.97	0.0443	6,765	1.05	3.10
VT-12	7,460	0.91	0.0416	6,675	1.11	4.53

TABLE 6

Summary of Geometric Parameters and Collapse Pressures for Series ET Models

Model	p_{exp} psi	R_{1_0} in.	h_a in.	$p'_E = 0.84\sqrt{E_s E_t}\left(h_a/R_{1_0}\right)^2$ psi	p_{exp}/p'_E	$\beta = 0.91\, L_i / \sqrt{R\, h_{min}}$
ET- 1	377	2.05	0.0133	383	0.98	1.72
ET- 2	360	2.21	0.0141	370	0.97	1.81
ET- 3	318	2.39	0.0135	290	1.10	1.95
ET- 4	310	2.53	0.0138	270	1.15	2.07
ET- 5	268	2.44	0.0118	217	1.26	2.78
ET- 6	365	2.22	0.0133	326	1.12	2.56
ET- 7	350	1.78	0.0117	387	0.90	3.10
ET- 8	246	1.80	0.0097	262	0.94	3.86
ET- 9	357	1.80	0.0122	412	0.87	3.92
ET-10	295	2.01	0.0119	320	0.92	4.40
ET-11	375	2.02	0.0119	314	1.19	4.90
ET-12	282	1.92	0.0089	195	1.46	6.80
ET-12A	223	2.29	0.0090	138	1.62	6.50
ET-13	460	1.79	0.0117	386	1.19	7.75

REFERENCES

1. Timoshenko, S., "Theory of Elastic Stability," McGraw-Hill Book Co., Inc., New York (1936).

2. Fung, Y. C. and Seckler, E. E., "Instability of Thin Elastic Shells," Proceedings of the First Symposium on Naval Structural Mechanics (1960).

3. Krenzke, M. A. and Kiernan, T. J., "Tests of Stiffened and Unstiffened Machined Spherical Shells under External Hydrostatic Pressure," David Taylor Model Basin Report 1741 (Aug 1963).

4. Klöppel, K. and Jungbluth, O., "Beitrag zum Durchchlagsproblem Dunwandieger Kugelschalen (Versuche and Bemessungsformeln). (Contribution to the Durchechlag Problem in Thin-Walled Spherical Shells (Experiments and Design Formulas)," Der Stahlbau, Jahrg. 22, Heft 6, Berlin (1953).

5. Thompson, J.M.T., "The Elastic Instability of Spherical Shells," Ph.D. Dissertation, Cambridege University (Sep 1961).

6. Wedellsborg, B. W., "Critical Buckling Load on Large Spherical Shells," Journal of the Structural Division, American Society of Civil Engineers, Vol. 88, No. ST1 (Feb 1962).

7. Krenzke, M. A., "Tests of Machined Deep Spherical Shells under External Hydrostatic Pressure," David Taylor Model Basin Report 1601 (May 1962).

8. Krenzke, M. A., "The Elastic Buckling Strength of Near-Perfect Deep Spherical Shells with Ideal Boundaries," David Taylor Model Basin Report 1713 (Jul 1963).

9. Bijlaard, P. P., "Theory and Tests on the Plastic Stability of Plates and Shells," Journal of the Aeronautical Sciences, Vol. 16, No. 9 (Sep 1949).

10. Krenzke, M. A. and Kiernan, T. J., "Elastic Stability of Near-Perfect Shallow Spherical Shells," AIAA Journal, Vol. 1, No. 12, p. 3855 (Dec 1963).

11. Tsien, H. S., "A theory for the Buckling of Thin Shells," Journal of the Aeronautical Sciences, Vol. 9, No. 10 (Aug 1942).

12. Kaplan, A. and Fung, Y. C., "A Non-Linear Theory of Bending and Buckling of Thin Elastic Shallow Spherical Shells," National Advisory Committee for Aeronautics TN 3212 (Aug 1954).

13. Homewood, R. H. et. al., "Experimental Investigation of the Buckling Instability of Monocoque Shells," Experimental Mechanics, Vol. 1, No. 3, p. 88 (Mar 1961).

14. Budiansky, B., "Buckling of Clamped Shallow Spherical Shells," Proceedings of the I.V.T.A.M. Symposium of the Theory of Thin Elastic Shells, North Holland Publishing Company, Amsterdam, p. 64 (1960).

15. Weinitschke, H., "On the Stability Problem for Shallow Spherical Shells," Journal of Mathematics and Physics, Vol. 38, No. 4, p. 209 (Jun 1960).

16. Thurston, G. A., "A Numerical Solution of the Non-Linear Equations for Axisymmetric Bending of Shallow Spherical Shells," Journal of Applied Mechanics, Vol. 28, No. 4, p. 557 (Dec 1961).

17. Huang, N. C., "Unsymmetric Buckling of Thin Shallow Spherical Shells," Technical Report 15, Harvard University (Mar 1963).

18. Weinitschke, H., "Asymmetric Buckling of Clamped Shallow Spherical Shells," National Advisory Space Administration TND-1510, p. 481 (Dec 1962).

Unclassified

Security Classification

DOCUMENT CONTROL DATA - R&D

(Security classification of title, body of abstract and indexing annotation must be entered when the overall report is classified)

1. ORIGINATING ACTIVITY (Corporate author) David Taylor Model Basin	2a. REPORT SECURITY CLASSIFICATION Unclassified 2b. GROUP

3. REPORT TITLE

THE EFFECT OF INITIAL IMPERFECTIONS ON THE COLLAPSE STRENGTH OF SPHERICAL SHELLS

4. DESCRIPTIVE NOTES (Type of report and inclusive dates)

Final

5. AUTHOR(S) (Last name, first name, initial)

Krenzke, Martin A., and Kiernan, Thomas J.

6. REPORT DATE February 1965	7a. TOTAL NO. OF PAGES 36	7b. NO. OF REFS 18
8a. CONTRACT OR GRANT NO. b. PROJECT NO. S-R011 01 01 c. d.	9a. ORIGINATOR'S REPORT NUMBER(S) 1757 9b. OTHER REPORT NO(S) (Any other numbers that may be assigned this report)	

10. AVAILABILITY/LIMITATION NOTICES

11. SUPPLEMENTARY NOTES	12. SPONSORING MILITARY ACTIVITY Bureau of Ships

13. ABSTRACT

DD FORM 1 JAN 64 1473

(ENCLOSURE 1)

Security Classification

14. KEY WORDS	LINK A		LINK B		LINK C	
	ROLE	WT	ROLE	WT	ROLE	WT
Spherical Shells initial imperfections collapse strength elastic behavior inelastic behavior buckling instability external hydrostatic pressure uniform pressure						

INSTRUCTIONS

1. **ORIGINATING ACTIVITY:** Enter the name and address of the contractor, subcontractor, grantee, Department of Defense activity or other organization *(corporate author)* issuing the report.

2a. **REPORT SECURITY CLASSIFICATION:** Enter the overall security classification of the report. Indicate whether "Restricted Data" is included. Marking is to be in accordance with appropriate security regulations.

2b. **GROUP:** Automatic downgrading is specified in DoD Directive 5200.10 and Armed Forces Industrial Manual. Enter the group number. Also, when applicable, show that optional markings have been used for Group 3 and Group 4 as authorized.

3. **REPORT TITLE:** Enter the complete report title in all capital letters. Titles in all cases should be unclassified. If a meaningful title cannot be selected without classification, show title classification in all capitals in parenthesis immediately following the title.

4. **DESCRIPTIVE NOTES:** If appropriate, enter the type of report, e.g., interim, progress, summary, annual, or final. Give the inclusive dates when a specific reporting period is covered.

5. **AUTHOR(S):** Enter the name(s) of author(s) as shown on or in the report. Enter last name, first name, middle initial. If military, show rank and branch of service. The name of the principal author is an absolute minimum requirement.

6. **REPORT DATE:** Enter the date of the report as day, month, year, or month, year. If more than one date appears on the report, use date of publication.

7a. **TOTAL NUMBER OF PAGES:** The total page count should follow normal pagination procedures, i.e., enter the number of pages containing information.

7b. **NUMBER OF REFERENCES:** Enter the total number of references cited in the report.

8a. **CONTRACT OR GRANT NUMBER:** If appropriate, enter the applicable number of the contract or grant under which the report was written.

8b, 8c, & 8d. **PROJECT NUMBER:** Enter the appropriate military department identification, such as project number, subproject number, system numbers, task number, etc.

9a. **ORIGINATOR'S REPORT NUMBER(S):** Enter the official report number by which the document will be identified and controlled by the originating activity. This number must be unique to this report.

9b. **OTHER REPORT NUMBER(S):** If the report has been assigned any other report numbers *(either by the originator or by the sponsor)*, also enter this number(s).

10. **AVAILABILITY/LIMITATION NOTICES:** Enter any limitations on further dissemination of the report, other than those imposed by security classification, using standard statements such as:

(1) "Qualified requesters may obtain copies of this report from DDC."

(2) "Foreign announcement and dissemination of this report by DDC is not authorized."

(3) "U. S. Government agencies may obtain copies of this report directly from DDC. Other qualified DDC users shall request through

_____."

(4) "U. S. military agencies may obtain copies of this report directly from DDC. Other qualified users shall request through

_____."

(5) "All distribution of this report is controlled. Qualified DDC users shall request through

_____."

If the report has been furnished to the Office of Technical Services, Department of Commerce, for sale to the public, indicate this fact and enter the price, if known.

11. **SUPPLEMENTARY NOTES:** Use for additional explanatory notes.

12. **SPONSORING MILITARY ACTIVITY:** Enter the name of the departmental project office or laboratory sponsoring *(paying for)* the research and development. Include address.

13. **ABSTRACT:** Enter an abstract giving a brief and factual summary of the document indicative of the report, even though it may also appear elsewhere in the body of the technical report. If additional space is required, a continuation sheet shall be attached.

It is highly desirable that the abstract of classified reports be unclassified. Each paragraph of the abstract shall end with an indication of the military security classification of the information in the paragraph, represented as *(TS)*, *(S)*, *(C)*, or *(U)*.

There is no limitation on the length of the abstract. However, the suggested length is from 150 to 225 words.

14. **KEY WORDS:** Key words are technically meaningful terms or short phrases that characterize a report and may be used as index entries for cataloging the report. Key words must be selected so that no security classification is required. Identifiers, such as equipment model designation, trade name, military project code name, geographic location, may be used as key words but will be followed by an indication of technical context. The assignment of links, roles, and weights is optional.